AIP | Advances

Si and C emission into the oxide layer during the oxidation of silicon carbide and its influence on the oxidation rate

Yasuto Hijikata, Ryosuke Asafuji, Ryotaro Konno, Yurie Akasaka, and Ryo Shinoda

Citation: AIP Advances **5**, 067128 (2015); doi: 10.1063/1.4922536
View online: http://dx.doi.org/10.1063/1.4922536
View Table of Contents: http://scitation.aip.org/content/aip/journal/adva/5/6?ver=pdfcov
Published by the AIP Publishing

Si and C emission into the oxide layer during the oxidation of silicon carbide and its influence on the oxidation rate

Yasuto Hijikata,[a] Ryosuke Asafuji, Ryotaro Konno, Yurie Akasaka, and Ryo Shinoda

Division of Mathematics Electronics and Information Sciences, Graduate School of Science and Engineering, Saitama University, 255 Shimo-Okubo, Sakura-ku, Saitama-shi, Saitama 338-8570, Japan

(Received 25 March 2015; accepted 3 June 2015; published online 10 June 2015)

Si and C emission into the oxide layer during the oxidation of silicon carbide and SiO_2 growth on the oxide surface were experimentally confirmed from depth profiles of oxidized HfO_2/SiC structures. With longer oxidation times, surface SiO_2 growth transitioned to oxide/SiC interface growth. The influence of Si and C emission on the oxidation rate was investigated by real-time measurements of the oxide growth rate. Experimental observations of annealing-inserted oxidation and two-temperature oxidation indicated that the emission suppressed the oxidation rate. [http://dx.doi.org/10.1063/1.4922536]

Silicon carbide (SiC) is an attractive wide bandgap semiconductor material because it has superior physical properties for power device applications and because its native oxide is SiO_2, which is utilized as an insulator in metal-oxide-semiconductor field-effect-transistors (MOSFETs). Unfortunately, the prospective low on-resistance based on the material properties of SiC has not yet been realized in actual fabricated SiC-MOSFETs, especially for 4*H*-SiC.[1] This is believed to be caused by the low channel mobility, which is attributed to the high trap densities at and/or near the SiO_2/SiC interface.[2] Although fabrication processes that improve the interface characteristics, such as nitridation of the interface, have been developed, it is difficult to simultaneously maintain sufficient long-term reliability of the oxide.[3] Since the creation of interface layers and the characteristics of oxide layers should be closely related to the oxide growth mechanism, an improved understanding of the mechanism is very important.

We carried out real-time measurements of the oxide growth rate of SiC using an *in-situ* spectroscopic ellipsometer,[4–6] and showed that the oxide growth rates in the thin oxide regime are higher than those predicted from the linear-parabolic model, called the Deal-Grove (DG) model.[7] Ray *et al.* also pointed out that the measured oxide thicknesses deviate from those predicted by the DG model until a few tens of nm in thickness.[8] A similar deviation in the thin oxide region has also been observed in Si oxidation,[9] and has been considered to result from a reduction in the reaction rate at the Si–SiO_2 interface due to the accumulation of Si atoms emitted into the SiO_2 layer.[10] Based on this idea, we proposed an SiC oxidation model, called the 'Si and C emission model',[11] in which it was assumed that Si and C atoms are emitted from the SiO_2–SiC interface into the SiO_2 layer during oxidation and the interfacial oxidation rate is reduced if these atoms accumulate near the interface. To describe this initial deceleration process, we used an interfacial reaction rate that decreases as oxidation progresses, i.e.,[11]

$$k = k_0\left(1 - \frac{C_{\mathrm{Si}}^{\mathrm{I}}}{C_{\mathrm{Si}}^{0}}\right)\left(1 - \frac{C_{\mathrm{C}}^{\mathrm{I}}}{C_{\mathrm{C}}^{0}}\right), \tag{1}$$

where k_0, C^{I}, and C^0 are the initial interfacial reaction rate, the concentrations at the SiC–SiO_2

[a]E-mail: yasuto@opt.ees.saitama-u.ac.jp

interface, and the solubility limits in SiO_2, respectively. We calculated growth rates using the Si and C emission model, and the calculated growth rate curves exactly reproduced the observed results, even in the thin oxide regime.[11,12]

However, this model was not based completely on experimental evidence because the Si emission was theoretically deduced[11,13] and its direct observation has been unsuccessful. However, there is a hypothesis that Si vacancies formed by Si emission are the origin of the interface state density near the conduction band edge.[14] On the other hand, C emission has been observed on both the SiO_2[15,16] and SiC substrate sides.[17–19] It has been reported that C injection into the SiO_2 layer can be attributed to the interface state over a wide energy range,[20] and the injected C interstitials create C dimers/di-interstitials in the SiC layer, which gives rise to the interface state near the conduction band edge.[21,22] Furthermore, it has been assumed in the development of bipolar devices that C vacancies, which give rise to deep-level states called $Z_{1/2}$ centers, are filled with C interstitials that diffuse into the SiC layer during oxidation.[17–19] It is believed that such atomic emissions during oxidation can help explain device-killing defects.

In Si oxidation, obvious evidence of Si emission was obtained by oxidizing $HfO_2/SiO_2/Si$ structures.[23] After thermal oxidation of the structure, the accumulation of Si species on the HfO_2 surface was clearly observed by high-resolution Rutherford backscattering spectroscopy. Another uncertainty of the Si and C emission model is whether the accumulation of Si and C interstitials near the interface really reduce the oxidation rate, even if such accumulation occurs. In previous work involving Si oxidation, this deceleration phenomenon has been confirmed by observing the increase in the re-oxidation rate after Ar annealing, which was attributed to the diffusion of Si interstitials from the interface.[24]

In this letter, we describe the behavior of Si and C atoms during the oxidation of SiC by depth-profiling oxidized HfO_2/SiC structures using time-of-flight secondary ion mass spectroscopy (TOF-SIMS) and angle-resolved X-ray photoemission spectroscopy (AR-XPS). We attempted to observe the transient period from the initial step in which oxide growth on the oxide surface is predominant (i.e. *active oxidation* mode[25]) to the steady-state in which interfacial oxide growth is predominant (i.e. *passive oxidation* mode). Furthermore, real-time measurements of the re-oxidation rate after Ar annealing and two-temperature (two-step) oxidation were carried out to examine the reduction of the oxidation rate due to accumulation of Si and C interstitials near the interface.

Epitaxial wafers of 4*H*-SiC with an 8° off-oriented (0001) Si-face, *n*-type, and with a net donor concentration N_d–$N_a = 1 \times 10^{16}$ cm^{-3} were used in this study. 5.6-nm-thick HfO_2 films were grown by an electronic-beam evaporator. The surface roughness of the grown HfO_2 films, as measured by atomic force microscopy, was less than 0.4 nm, which is sufficient for TOF-SIMS analysis. The samples were oxidized in an infrared furnace at 1100ºC in a dry stable-isotope oxygen ($^{18}O_2$) atmosphere at 13 Pa for 1 or 10 min in an attempt to trace the oxidant behavior under active oxidation conditions. For comparison, a sample was also annealed in a high vacuum chamber (base pressure $<1 \times 10^{-5}$ Pa) at 1100ºC for 30 min. The samples were then analyzed by TOF-SIMS. The details on the TOF-SIMS measurements were presented elsewhere.[26] Another HfO_2/SiC structure was oxidized at 1100ºC and 100 kPa to observe the transition from the active oxidation mode to the passive oxidation mode. AR-XPS was performed to obtain depth profiles of the oxide films, which were grown by 1, 10, 60, or 180 min of oxidation. To confirm the suppression of the oxidation rate due to the accumulation of interstitials, real-time measurements of the re-oxidation rate after Ar annealing and of two-step oxidation were carried out using an *in-situ* spectroscopic ellipsometer. The SiC substrates used here were obtained from the same wafer mentioned above. For Ar annealing-inserted oxidation measurements, the oxidation was ceased when the oxide was grown to 10, 20, or 45 nm, then Ar annealing was carried out, and the oxidation was restarted. The oxidation temperature was fixed at 1150ºC, and the annealing temperature was 1150ºC or 1050ºC. When switching gases, the furnace was pumped to vacuum, and heating was ceased under vacuum in order to avoid the growth of carbon rich layer on the SiC surface. For the two-step oxidation measurements, the initial oxidation temperature was varied between 900 and 1200ºC, and the oxidation temperature of the second step was fixed at 1100ºC. The thickness at which the oxidation

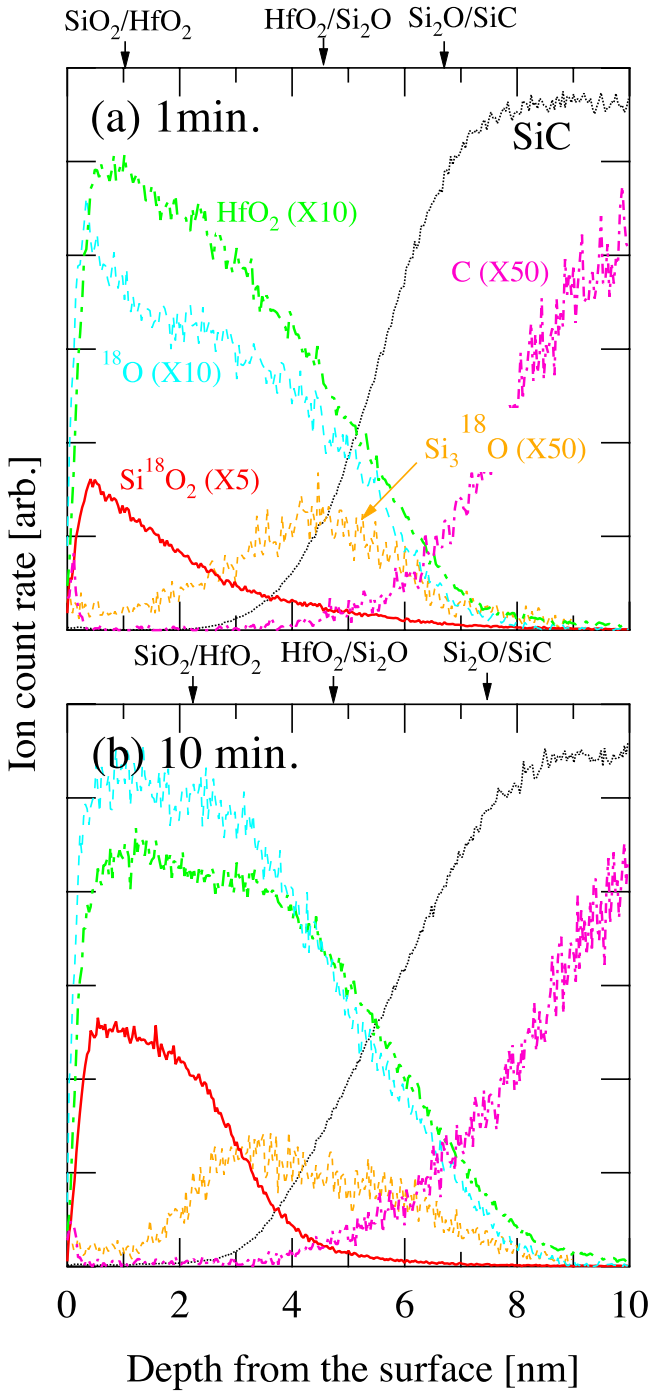

FIG. 1. Depth profiles of ^{18}O, SiC, HfO_2, C, $Si^{18}O_2$, and $Si_2{}^{18}O$ for 1 min oxidation (a) and 10 min oxidation (b).

temperature was switched was also fixed at 3 nm. The details of the oxide growth rate measurements were presented elsewhere.[5]

Figure 1 shows depth profiles of ^{18}O, SiC, $^{180}Hf^{16}O_2$, C, $Si_2{}^{18}O_5$ (equivalent to $Si^{18}O_2$), and $Si_2{}^{18}O$ (equivalent to a sub-oxide, i.e. Si^{1+} in the Ref. 27), for 1 min of oxidation (a) and 10 min of oxidation (b). Analysis of the annealed sample (not shown here) confirmed that no Si atoms were emitted into the HfO_2 layer. In contrast, the depth profiles of the oxidized samples clearly indicated that SiO_2 was grown near the HfO_2 surface. Moreover, the SiO_2 growth in the 10 min oxidized

sample progressed more, and the $Si^{18}O_2/HfO_2$ interface became more abrupt. These are strong indications of Si emission from the SiO_2–SiC interface into the SiO_2 layer during oxidation. Also, these results confirm that the emitted Si atoms diffuse outward toward the surface and are oxidized when they encounter oxygen from the gas phase. Under such oxidation conditions dominant to the active oxidation mode, little growth of SiO_2 occurs at the interface. Instead, only the sub-oxide grows at the interface. Furthermore, the amount of sub-oxide increases very slightly as oxidation progresses. Since the thickness of sub-oxide is determined by the diffusion length of Si interstitial (independent of oxidation time),[10] the thickness should become constant at the steady-state. In addition, the growth of sub-oxide is transitioned to the steady-state at the very early oxidation stage because the emitted Si interstitials are instantly oxidized near the interface, as revealed in the Si oxidation.[23] As shown in Fig. 1, it was found that in this oxidation stage, there were few C interstitials in the oxide. Since the ratio of C interstitial emitting into the SiC substrate to the density of C atoms in SiC is only the order of 10^{-10},[28] most of C interstitials are emitted into the oxide-side and diffuse up to the surface of oxide, then instantly evaporating toward the gas phase. As reported in the Refs. 15 and 16 in the case of ordinary pressure oxidation and thicker oxide, C interstitials with a higher concentration should exit in the oxide.

Figure 2 shows a photoemission spectrum in the O1s region for a 1 min oxidized sample (a) and the peak area ratio of $I(SiO_x)$ to $I(HfO_2)$ as a function of photoelectron take-off angle (θ; 0^o denotes parallel to the sample surface) for various oxidation times (b). As shown in Fig. 2(a), the spectrum is divided into two component peaks, which originate from HfO_2 at a binding energy of approximately 530 eV and from SiO_x around 532 eV. The dotted curves in Fig. 2(b) were obtained by curve-fitting using the layer attenuation model.[27] The SiO_x thicknesses derived from the curve-fits are shown in Table I. Note that the multilayer structure used for the analysis was X_2/HfO_2 (2.8 nm)/X_1/SiC.

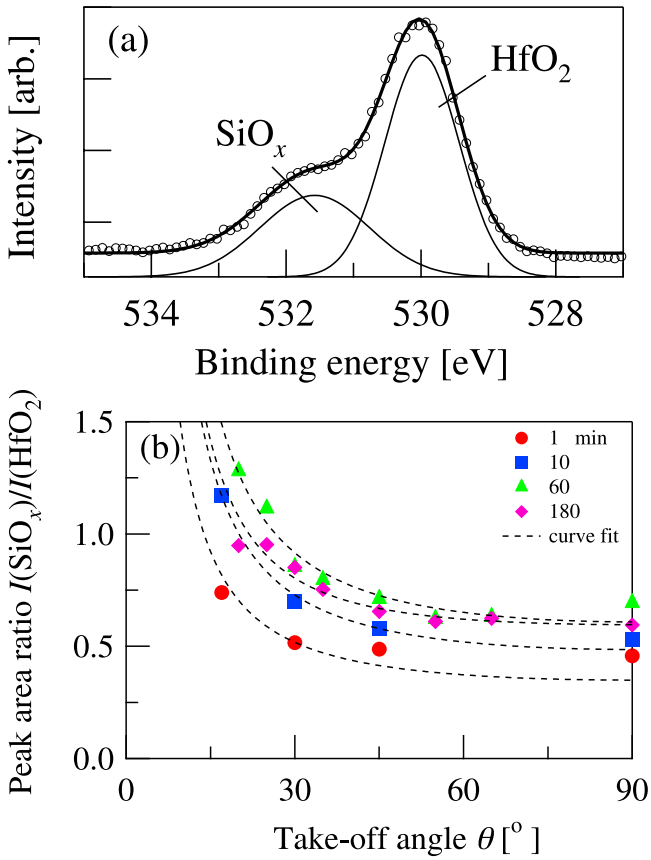

FIG. 2. Photoemission spectra in the O1s region for a 1 min oxidized sample (a) and the peak area ratio of $I(SiO_2)$ to $I(HfO_2)$ as a function of photoelectron take-off angle ($\theta = 0^o$ denotes parallel to the sample surface) for various oxidation times (b).

TABLE I. Thickness of the multi-layer structure.

t_{ox} [min.][a]	d_1 [nm][b]	d_2 [nm][b]
1	~0	0.19
10	~0	0.25
60	0.14	0.31
180	2.8	0.27

[a] t_{ox} is the oxidation time.
[b] d_n is the thickness of SiO_x at nth layer in X_2/HfO_2 (2.8 nm)/X_1/SiC structure.

Although analysis of samples oxidized for less than 10 min indicated Si oxide growth on the HfO_2 surface, after oxidation for 60 min caused the oxide growth to predominantly occur at the oxidation interface. Therefore, the active oxidation mode transitions to the passive oxidation mode as the oxidation of SiC substrate progresses. This is similar to Si oxidation.[29] In comparison to the case of low-pressure oxidation, thickness of the SiO_2 layer at ordinary pressure is smaller. The reason why the lowering of the oxygen pressure enhances the SiO_2 growth is probably due to a larger diffusivity of Si interstitial.

Figure 3(a) shows the oxide growth rate as a function of oxide thickness, both without annealing, and before and after Ar annealing at 1150°C for 2 h. The unfilled and filled symbols denote

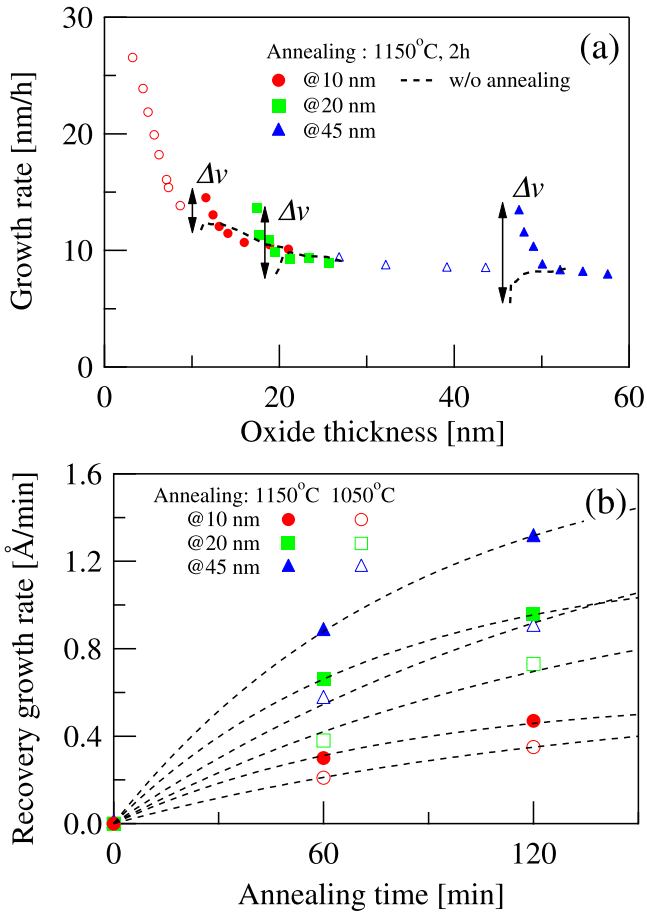

FIG. 3. (a) Oxide growth rates with and without Ar annealing insertion as a function of oxide thickness. The annealing temperature was 1150°C, the annealing time was 2 h, and the annealed oxide thicknesses were 10, 20, and 45 nm. (b) Annealing time dependence of recovery rates. Annealing temperatures were 1050 and 1150°C. The dotted curves denote curves fit using Eq. (2).

TABLE II. Parameters for Eq. (2), obtained from curve fitting.

d_a [nm][a]	Δv_{max} at 1150 °C [nm/min.]	τ at 1150 °C [min.]	Δv_{max} at 1050 °C [nm/min.]	τ at 1050 °C [min.]
10	0.059	80	0.061	141
20	0.119	74	0.122	142
45	0.175	86	0.171	156

[a]d_a is the annealed thickness.

growth rates before and after Ar annealing, respectively. As shown in the figure, the growth rates were increased by Ar annealing. Furthermore, the larger the annealed thickness, the larger the increase in growth rate. Figure 3(b) shows the recovery rate (Δv; shown in Fig. 3(a)) as a function of annealing time at 1150°C or 1050°C. Here, we assume that Δv increases exponentially to the maximum recovery rate (Δv_{max}) with a recovery time constant τ, i.e.,

$$\Delta v = \Delta v_{max} (1 - \exp(-t/\tau)) . \quad (2)$$

The dotted lines in the figure denote curves fitted using Eq. (2). Table II shows all of the values of Δv_{max} and τ obtained in this study. From the table, Δv_{max} increases with increasing annealed thickness, and is almost independent of annealing temperature. Conversely, τ decreases with increasing annealing temperature, and is almost independent of annealed thickness. According to the Si and C emission model, the recovery of oxidation rate due to annealing can be explained by the diffusion of Si and/or C interstitials from the oxidizing interface. Taking diffusion theory into account, this model is reasonable because Δv_{max} should depend only on the interstitial concentration before annealing and τ should depend only on the diffusion coefficient of the interstitial, which depends not on oxide thickness but on temperature.

Figure 4 shows the oxide thickness dependence of the oxide growth rate at various initial oxidation temperatures, as obtained from the two-step oxidation experiments. It is very interesting that a lower initial temperature leads to a higher growth rate in the second step, even though the second oxidation temperature and switching thickness are common between these oxidation sequences. Furthermore, for all initial temperatures, the growth rates converged to a common rate after a few tens of nm of growth in the second step. According to the Si and C emission model, the oxidation rate for the interface reaction rate-limiting step is determined by k_0 and the ratio C^I/C^0, as shown in Eq. (1). Since the k_0 and C^0 values are common after the second oxidation step begins, the

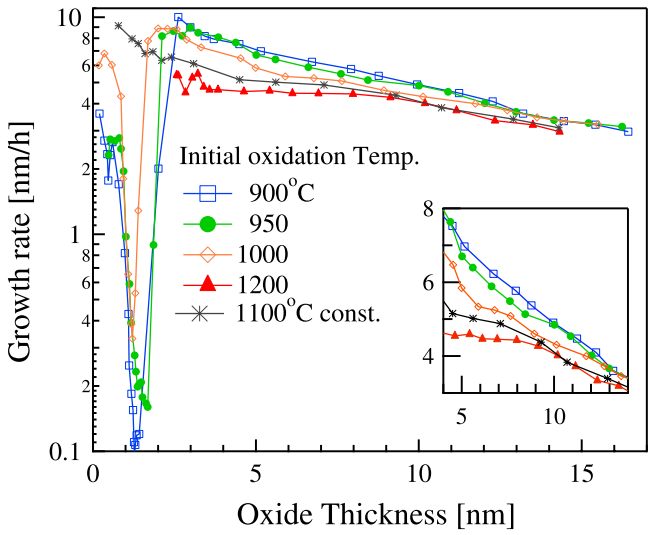

FIG. 4. Oxide growth rates as a function of oxide thickness at various initial oxidation temperatures. The second step oxidation temperature was 1100°C for all samples. The inset denotes growth rate data restricted to the second oxidation.

difference in the oxidation rates is probably due to the difference in C^I. The lower C^0 should lead to a lower C^I at the end of the initial oxidation and, therefore, the lower initial oxidation temperature (i.e. lower C^0) accounts for the higher oxidation rate of the second oxidation. In addition, the reason why growth rates converge to a common rate is that, after oxide growth is sufficiently progressed, each C^I value approaches an intrinsic one for the second oxidation temperature.

In summary, we attempted to experimentally examine two phenomena related to the SiC oxidation mechanism. One was Si and C emission into the oxide layer during the oxidation of SiC, which was investigated by obtaining depth profiles of oxidized HfO_2/SiC structures. With longer oxidation times, a transition from active oxidation mode to passive oxidation mode was also observed. The hypothesis in the Si and C emission model that emitted Si and C interstitials suppress the oxidation rate was confirmed by two different real-time observations of oxide growth on SiC, i.e. variation of the re-oxidation rate after Ar annealing and that of the oxidation rate during two-step oxidation. These experimental results strongly support the validity of the Si and C emission model.

ACKNOWLEDGEMENT

This work was partly supported by a Grant-in-Aid for Scientific Research (24560365) from the Japan Society for the Promotion of Science.

[1] H. Matsunami, Jpn. J. Appl. Phys. **43**, 6835 (2004).
[2] G. Y. Chung, C. C. Tin, J. R. Williams, K. McDonald, R. K. Chanana, A. Weller, S. T. Pantelides, L. C. Feldman, O. W. Holland, M. K. Das, and J. W. Palmour, IEEE Electron Device Lett. **22**, 176 (2001).
[3] J. Rozen, S. Dhar, M. E. Zvanut, J. R. Williams, and L. C. Feldman, J. Appl. Phys. **105**, 124506 (2009).
[4] T. Yamamoto, Y. Hijikata, H. Yaguchi, and S. Yoshida, Jpn. J. Appl. Phys. **47**, 7803 (2008).
[5] K. Kouda, Y. Hijikata, H. Yaguchi, and S. Yoshida, J. Appl. Phys. **112**, 024502 (2012).
[6] D. Goto, Y. Hijikata, S. Yagi, and H. Yaguchi, J. Appl. Phys. **117**, 095306 (2015).
[7] B. E. Deal and A. S. Grove, J. Appl. Phys. **36**, 3770 (1965).
[8] E. A. Ray, J. Rozen, S. Dhar, L. C. Feldman, and J. R. Williams, J. Appl. Phys. **103**, 023522 (2008).
[9] H. Z. Massoud, J. D. Plummer, and E. A. Irene, J. Electrochem. Soc. **132**, 2685 (1985).
[10] H. Kageshima, K. Shiraishi, and M. Uematsu, Jpn. J. Appl. Phys. Part 2 **38**, L971 (1999).
[11] Y. Hijikata, H. Yaguchi, and S. Yoshida, Appl. Phys. Express **2**, 021203 (2009).
[12] Y. Hijikata, S. Yagi, H. Yaguchi, and S. Yoshida, in *Physics and Technologies of Silicon Carbide Devices*, edited by Y. Hijikata (InTech, 2013), p. 181 Chap. 7.
[13] T. Christen, A. Ioannidis, and C. Winkelmann, J. Appl. Phys. **117**, 084501 (2015).
[14] D. J. Meyer, P. M. Lenahan, and A. J. Lelis, Appl. Phys. Lett. **86**, 023503 (2005).
[15] K. C. Chang, N. T. Nuhfer, L. M. Porter, and Q. Wahab, Appl. Phys. Lett. **77**, 2186 (2000).
[16] C. Radtke, F. C. Stedile, G. V. Soares, C. Krug, E. B. O. da Rosa, C. Driemeier, I. J. R. Baumvol, and R. P. Pezzi, Appl. Phys. Lett. **92**, 252909 (2008).
[17] T. Hiyoshi and T. Kimoto, Appl. Phys. Express **2**, 091101 (2009).
[18] L. S. Løvlie and B. G. Svensson, Phys. Rev. B **86**, 075205 (2012).
[19] T. Miyazawa and H. Tsuchida, J. Appl. Phys. **113**, 083714 (2013).
[20] V. V. Afanas'ev, M. Bassler, G. Pensl, and M. J. Schulz, Phys. Status Solidi A **162**, 321 (1997).
[21] A. Gavrikov, A. Knizhnik, A. Safonov, A. Scherbinin, A. Bagatur'yants, B. Potapkin, A. Chatterjee, and K. Matocha, J. Appl. Phys. **104**, 093508 (2008).
[22] X. Shen and S. T. Pantelides, Appl. Phys. Lett. **98**, 053507 (2011).
[23] Z. Ming, K. Nakajima, M. Suzuki, K. Kimura, M. Uematsu, K. Torii, S. Kamiyama, Y. Nara, and K. Yamada, Appl. Phys. Lett. **88**, 153516 (2006).
[24] J. Farjas and P. Roura, J. Appl. Phys. **102**, 054902 (2007).
[25] N. S. Jacobson and D. L. Myers, Oxid. Met. **75**, 1 (2011).
[26] Y. Hijikata, Y. Akasaka, S. Yagi, and H. Yaguchi, Mater. Sci. Forum **778-780**, 553 (2014).
[27] L. I. Johansson, C. Virojanadara, Th. Eickhoff, and W. Drube, Surf. Sci. **529**, 515 (2003).
[28] K. Kawahara, J. Suda, and T. Kimoto, J. Appl. Phys. **111**, 053710 (2012).
[29] T. Engel, Surf. Sci. Rep. **18**, 93 (1993).